Revista Ingeniería de Construcción RIC
Vol 37 Nº3 2022 www.ricuc.cl
DOI: 10.7764/RIC.00046.21

ENGLISH VERSION

Experimental determination of stress-strain characteristics of very high strength unconfined concrete in compression including comparison with normal and high strength concrete

Determinación experimental de las características de tensión deformación del hormigón de muy alta resistencia no confinado en compresión, incluida la comparación con hormigón de resistencias normal y alta

Ojha, P.N. * *http://orcid.org/0000-0003-1754-4488*
Singh, Brijesh * *http://orcid.org/0000-0002-6512-1968*
Singh, Pranay *[1] *http://orcid.org/0000-0001-6169-9482*
Mittal, Piyush * *http://orcid.org/0000-0002-1994-0946*
Singh, Abhishek * *http://orcid.org/0000-0002-2343-5934*

Fecha de recepción: 21-06-2022
Fecha de aceptación: 04-10-2022
Fecha de publicación:02-12-2022
PAG 435-449

* *National Council For Cement and Building Materials, Faridabad –INDIA*

Abstract

Indian standard Code-IS:456-2000 and Eurocode EC:02-2004 for the design of the concrete structure is limited to the concrete with compressive strength of 55 MPa and 90 MPa respectively. For defining the stress block parameters and for the design of concrete structures using Very high strength concrete (100 MPa to 150MPa); a well-defined stressstrain behavior becomes necessary, particularly the experimental values for the strain at peak stress and ultimate strain capacity. The presents study attempts to cater to these needs by experimentally evaluating the unconfined stressstrain behavior of nine cylindrical specimens with a compressive strength between 100 MPa to 150 MPa, in a servocontrolled (Strain-controlled) compression testing machine. The strain values recorded at peak stress for 100 MPa and 150 MPa concrete are approximately 3000 microstrains and 3500 microstrains respectively. Compared to normal and high-strength concrete, the rising limb of the curves for VHSC (Very high strength concrete) is much steeper and approaches a straight path, also the strain at peak stress and ultimate strain coincide, depicting a negligible post-peak strain hardening region. LVDT and compressometer gave different strains for the same load and specimen. This signifies the role of the gauge length ratio used in these strain measuring devices.

Keywords: *Very high strength concrete; compressive strength; Stress-Strain Curve; LVDT; compressometer.*

[1] ***Correspondence author:***
National Council For Cement and Building Materials, Faridabad –INDIA
Email singhpranay157@gmail.com

DOI: 10.7764/RIC.00046.21

Resumen

Las Norma India IS:456-2000 y europea EC:02-2004 para el diseño de estructuras de hormigón se limitan al hormigón con resistencia a la compresión de 55 MPa y 90 MPa respectivamente. Para definir los parámetros del bloque de tensión y para el diseño de estructuras de hormigón utilizando hormigón de muy alta resistencia (100 MPa a 150MPa) es necesario contar con un comportamiento tensión-deformación bien definido y, especialmente, con los valores experimentales para la deformación en la tensión máxima y la capacidad de deformación última. El presente estudio intenta satisfacer estas necesidades mediante la evaluación experimental del comportamiento a la tensión-deformación de nueve probetas cilíndricas de hormigón no confinado sometidas a una compresión entre 100 MPa y 150 MPa, en una máquina de ensayos a la compresión servo-controlada (controlada por tensión). Los valores de deformación registrados para el esfuerzo máximo del hormigón de 100 MPa y 150 MPa fueron de alrededor de 3.000 y 3.500 micro deformaciones respectivamente. En comparación con el hormigón normal y de alta resistencia, el tramo ascendente de las curvas para el hormigón de muy alta resistencia es mucho más pronunciado y se aproxima a una trayectoria recta, además coinciden la deformación en el esfuerzo máximo y la deformación última, representando un área insignificante de endurecimiento por deformación posterior al pico. El Transformador Diferencial de Variación Lineal (LVDT) y el compresómetro mostraron diferentes deformaciones para la misma probeta y carga. Esto demuestra el rol de la relación de la longitud de calibre utilizada en estos dispositivos de medición de tensión.

Palabras clave*: Hormigón de muy alta resistencia; resistencia a la compresión; curva tensión-deformación; Transformador Diferencial de Variación Lineal (LVDT); compresometro.*

1. Introduction

The demand for higher strength concrete is increasing rapidly in the construction industry. Modern skyscrapers, bridges, etc. require a much higher strength concrete. Also, with the available literature and past studies (Campos et al., 2020), it is possible to design higher-strength concrete much more easily than earlier. Studies are also available for making high to very high strength concrete with the indigenous material (Arora et al., 2017) available in the Indian subcontinent. But the primary step in designing any structure requires a better understanding of the material behavior, and the existing design parameters presented in Standard codes are getting redundant and require major updates for very high strength concrete. These design parameters are directly linked to the stress-strain characteristics of the concrete (Singh et al., 2020). The terms "normal strength concrete", "high strength concrete" and "very high strength concrete" are relative and require a clear demarcation for better understanding and standardized citation. (Zeng et. al., 2020) categorized concrete based on its compressive strength as Normal strength concrete up to 50 MPa, High strength concrete as 50 MPa to 100 MPa, and ultrahigh-strength concrete above 100 MPa. (Baduge et al., 2018) classified any concrete having compressive strength above 100 MPa as very-high strength concrete. (Kwan et al. 1995) considered the concrete with compressive strength above 100 MPa as very-high strength concrete. Based on the presented literature and the suitability with the meaning, normal strength concrete will refer to the concrete with compressive strength up to 50 MPa. High strength concrete refers to concrete with 50 MPa to 100 MPa and very high strength concrete will denote concrete having a compressive strength of 100 MPa to 150 MPa.

The stress-strain behavior of concrete varies largely with the increase in the compressive strength (Singh et al., 2020). Values of the strain at peak stress and the ultimate strain adopted by IS456 hold good only up to concrete grade M50. The strain values adopted by the Eurocode better represent the actual behavior of very high-strength concrete. But it also fails to represent the concrete above M90. (Singh et al. 2020), studied the stress-strain characteristics of high strength unconfined concrete and suggested some important changes in the existing Indian codes. Authors experimentally derived the stress-strain curves for the concrete having the cube compressive strength in the range of 45 Mpa TO 106 Mpa. The present study presents the stress-strain curves for the concrete above 100 MPa up to 140 Mpa. Some of the recent studies on high to very high strength concrete suggests better short-term mechanical properties (Arora et al., 2016). Also, (Singh et al., 2022), (Singh et al., 2021), (Singh et al., 2021) in their studies have presented the parameters, empirical equation along with experimental validation for the shear as well as the flexural design of High strength concrete. (Habeeb et al., 2019), (Habeeb et al., 2021), studied the punching shear in flat slabs made with Lightweight aggregate concrete having compressive strength up to 43 MPa.

DOI: 10.7764/RIC.00046.21

(Ojha et al., 2021), (Ojha et al., 2020) performed a series of experiments to evaluate the creep and shrinkage properties of high-rise buildings. (Arora et al., 2020) evaluated the modulus of elasticity of the high-strength concrete made using granite and calc-granulite aggregates. (Patel et al., 2020) studied the fracture properties of high-strength concrete. Studies (Oztekin et al., 2003), (Attard and Stewart, 1998) also suggest that rectangular stress block parameters for normal strength concrete can not be applied for the higher strength concrete. (Arora et al., 2019) studied the stress-strain behavior of high-strength plain and fiber reinforced concrete. The author presented stress-strain curves for normal and high strength concrete measured using LVDT and compressmeter. As presented here, extensive literature is available for normal and high strength concrete. Such literature on VHSC is limited.

VHSC has a very dense and homogeneous cement matrix as compared to conventional normal-strength or even highstrength concretes, as a consequence it has excellent mechanical and durability performance (Azmee and Shafiq, 2018), (AlZwainy et al., 2016). The uniform microstructure is the result of both physical and chemical factors (Sorelli et al., 2008), (De Larrard and Sedran, 1994). Physical factors such as maximizing particle packing by using a combination of materials with wider particle size distribution. Chemical factors such as secondary C-S-H formation because of abundant mineral admixture present, assisted by elevated curing which accelerates the hydration and pozzolanic reaction of mineral admixtures. (Richrad and Cheyrezy, 1995). Also, as there is less space available for the formation of C–S–H in VHSC, it has a high density characterized by intrinsic higher stiffness and hardness compared to conventional concrete's low-density C–S–H. Additionally, the use of a low water binder ratio along with low CH crystals as they are depleted during pozzolanic reaction results in a less porous interfacial transition zone (ITZ) (Chan and Chu, 2004), (Shi, 1996). It is well established that ITZ is the weakest link and reason for failure in conventional concrete, however in VHSC ITZ is almost as dense as its cement matrix leading to enhanced mechanical properties (Schmidt and Fehling, 2007), (Ojha et al., 2020). Despite several advantages of VHSC over conventional concrete, its use is limited due to constraints like high cost, limited design codes, and nonstandardized production methodology.

The current study primarily focuses on the stress-strain behavior of VHSC along with its mechanical properties. The obtained stress-strain characteristics of VHSC are compared with existing codes. In the subsequent sections, concrete making materials, mix design details, as well as experiential procedures, have been presented in the detail. In the results section, a total of 12 stress-strain curves are presented for the concrete with cylindrical compressive strength varying between 30 MPa to 140 MPa, sourced from the literature and the experiments. The variation in the strain measurement with the LVDT and compressometer is also discussed.

2. Materials

2.1 Cementitious Materials

Properties of VHSC are highly dependent on the type of material used in its production. In this study cementitious material with a broad range of particle size distribution has been selected which leads to a higher packing density of concrete. The physical and chemical properties of cementitious material are given in (Table 1) and (Table 2) respectively. The particle size distribution of all solid materials is given in (Figure 1) (Ojha et al., 2020). Cementitious Materials used in the study are OPC 53G, GGBS, Flyash, ultrafine GGBS, and Silica fume conforming to IS 269: 2015, IS 16714:2015, IS 3812, IS 16715:2015, IS 15388 respectively. Nano-silica was also used to fill the pores of Nano-size. Similarly, to increase the packing density of solid materials, three different types of aggregates are used namely Quartz sand, Ground Quartz, and River sand.

Table 1. *Physical properties of materials (Ojha et al., 2020)*

S. No.	Properties	Cement	G.G.B.S	Flyash	UFGGBS	Silica Fume	Nano Silica
1.	Fineness(m^2/kg)	323	400	310	2026	16701	24000
2.	Specific Gravity	3.15	2.93	2.28	2.88	2.28	2.21

DOI: 10.7764/RIC.00046.21

Table 2. *Chemical properties of materials*

S. No.	Properties	Cement	G.G.B.S	Flyash	UFGGBS	Silica Fume
1	Loss of Ignition (LOI)	2.3	0.33	0.4	0.17	2.73
2	Silica (SiO_2)	20.71	34.41	60.95	33.05	85.03
3	Iron oxide (Fe_2O_3)	4.08	1.18	5.7	0.58	-
4	Aluminium oxide (Al_2O_3)	5.15	18.45	26.67	20.40	-
5	Calcium oxide (CaO)	59.96	36.46	2.08	33.14	-
6	Magnesium oxide (MgO)	4.57	7.00	0.69	7.62	-
7	Sulphate (SO_3)	1.84	0.097	0.29	0.19	-
8	Na_2O	0.42	0.30	0.06	0.19	0.73
9	K_2O	0.56	0.37	1.46	0.58	2.96
10	Chlorides	0.012	0.022	0.009	0.016	-
11	Insoluble Residue	1.25	0.40	-	0.86	-

2.2 Aggregates

2.2.1 Ground Quartz

Ground Quartz having finer size particles was used as micro filler to increase the packing density of cement aggregate matrix. Its particle size ranges from 0.5 to 63 microns. Particle size distribution has been shown in (Figure 1). The majority of quartz grains are in the size range of 20µm to 30µm.

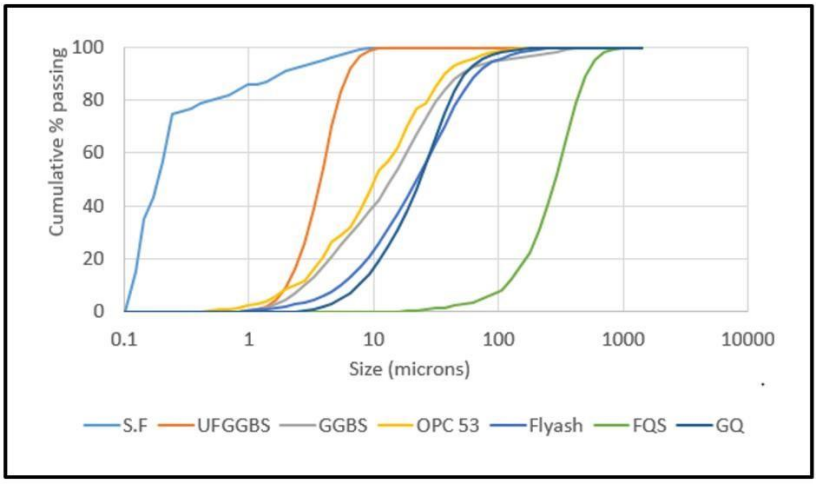

Figure 1. *Particle size distribution of materials (Ojha et al., 2020)*

2.2.2 Fine Quartz Sand

VHSC mixes were produced using quartz sand having a particle size ranging from 150 to 996 microns. Particle size distribution has been shown in (Figure 1). The majority of quartz grains are in the size range of 300µm to 600µm.

DOI: 10.7764/RIC.00046.21

2.2.3 Coarse Quartz sand

Coarse quartz sand used in this study has a particle size ranging from 1mm to 3mm. The microstructure of Coarse quartz sand by optical microscopy suggests that it has subhedral to anhedral quartz grains with sharp grain margins which are well-graded and homogenously distributed.

3. Experimental Procedures

3.1 Packing Density

In the present research, the ideal curve methodology has been adopted. In this method, materials are combined in such fractions that their combined grading lies close to a certain ideal curve to ensure the maximum packing density of solid materials (Ojha et al., 2020). We have used the ideal curve given by Modified Andreasen and Andersen equation as mentioned below in (Equation 1).

$$P(d) = \frac{d^q - {d_{min}}^q}{{d_{max}}^q - {d_{min}}^q} \quad (1)$$

Using an optimization algorithm based on the Least Squares Method (LSM) as given in (Equation 2), the amount of each solid material in the matrix is adjusted until an optimized fit with the least RSS value is obtained between the composed mix and the target curve given by Modified Andreasen and Andersen equation. To achieve the most optimum combinations with the least RSS values Excel Solver was used.

$$RSS = \sum_{i=1}^{n} (P_{mix}({D_i}^{i+1}) - P_{tar}({D_i}^{i+1}))^2 \quad (2)$$

Where P_{mix} is the composed mix and P_{tar} is the target grading.

Wet packing density was also determined using the below-mentioned equation referred to by (Ojha et.al., 2020). If the VHSC mix consists of several different materials denoted by α, β, γ, and so forth, ρ and R are solid density and volumetric ratio of the respective material. uw is the ratio of water to solid content. The solid volume of the cementitious materials V_c and wet packing density ϕ may be worked out from (Equation 3) and (Equation 4) mentioned below.

$$V_c = \frac{M}{\rho_w u_w + \rho_\alpha R_\alpha + \rho_\beta R_\beta + \rho_\gamma R_\gamma} \quad (3)$$

$$\phi = \frac{V_c}{V} \quad (4)$$

As per numerous researchers, the packing density of concrete is in the range given below in (Table 3)

.

DOI: 10.7764/RIC.00046.21

Table 3. *Packing density of different types of concrete (Schmidt and Fehling, 2007)*

Type of Concrete	Packing Density range
Normal strength Concrete	0.65 - 0.72
High Strength Concrete	0.72 – 0.8
Very high strength concrete	More than 0.8

3.2 Mix Design details

In the present study, the proportion of individual cementitious material was decided using the Modified Andreasen and Andersen equation. From mixes that were mathematically optimized based on their RSS value using an excel solver, seven final mixes were cast in the laboratory for a study on compressive strength, Stress-strain behavior, Modulus of elasticity, and split tensile strength. The details of the mix composition of these optimized mixes are given below. The total cementitious content used is 1000 kg/m^3. To attain better particle packing density, a combination of fine aggregates was used i.e. Ground quartz, Fine quartz sand, and coarse quartz sand. The nano-silica was used as 3% replacement for OPC content. (Table 4)

Table 4. *Packing density of different types of concrete (Schmidt and Fehling, 2007)*

Mix ID	OPC	GGBS	Flyash	UFGGBS	SF	NS	GQ	FQS	CQS	w/binder	Total Binder
Mix 1	582.0	200	0	100	100	18.0	292.6	498.4	371	0.17	1000
Mix 2	701.1	0	149.9	0	147	21.0	269.3	982.8	0	0.16	1000
Mix 3	640.0	218.2	0	0	140	19.2	275.8	1006.8	0	0.17	1000
Mix 4	655.3	109.1	94.6	0	139	19.7	271.2	989.8	0	0.17	1000
Mix 5	596.0	164.9	0	85.5	135	18.4	255.6	922.0	0	0.17	1000

3.3 Mix methodology

Adoption of an adequate Mixing methodology is vital as VHSC typically includes a limited amount of water and no coarse aggregate. Therefore, extra mixing energy is required in the case of VHSC, both to disperse the water and to overcome the low internal mixing action from the lack of coarse aggregate. A typical mixing process involves first charging the mixer with the dry components and ensuring that they are fully blended. Thereafter, the water and the liquid admixtures are added and dispersed. Mixing continues, sometimes for an extended period depending on the mixer energy input, until the VHSC changes from a dry powder into a fluid mixture. Dry mixing intends to ensure higher bulk density and lower moisture requirements.

3.4 Curing Regimes

The curing regime plays an important role in the strength development of VHSC as it influences the microstructure of VHSC which in turn affects its mechanical properties. Compared to the VHSC cured under ambient conditions, heat-treated specimens of VHSC show generally a denser microstructure that can lead to an increase in compressive strength and thus can improve the overall mechanical properties of VHSC. In the present study, samples have been steam cured at 90ºC and 100% RH followed by Standard curing till the age of testing.

3.5 Stress-strain behavior study and specimen size

The concrete specimens were tested at room temperature of 27±2ºC and relative humidity of 65% in a strain-controlled compression testing machine of 3000 KN capacity. Using a compressometer and LVDT the strains were recorded for the samples as shown in (Figure 3). To obtain the full stress vs strain curve, a rate of loading of 0.4 µm/sec was adopted.

DOI: 10.7764/RIC.00046.21

The specimens of sizes 100 mm in diameter and 200 mm in length were tested to obtain stress vs strain curves of all the VHSC mixes. Both ends of these concrete cylinders were ground to get a parallel finish. The specimen size was selected based on the maximum capacity of the equipment and the strength level of the concrete. The standard cylindrical specimen of 150 mm x 300 mm suggested by EC 02-2004 (European Standards En, 2004) and IS 456 (Bureau of Indian Standards, 2000) was also not considered since the maximum size of aggregate used was 4.75 mm. The specimen size suggested by European, Indian and other standards is for concrete with coarse aggregate size even up to 40 mm. Literature (Riedel et al., 2019) indicates that the mean cylinder compressive strength between 30 to 200 MPa shows very small coefficients of variation in compressive strength test results when the comparison is done for 100 mm and 150 mm specimen sizes. Compared with Normal Strength and High Performance Concrete, the effect of the specimen's geometry on the compressive strength is very small for UHPC. (Figure 2) shows the testing arrangement for the study.

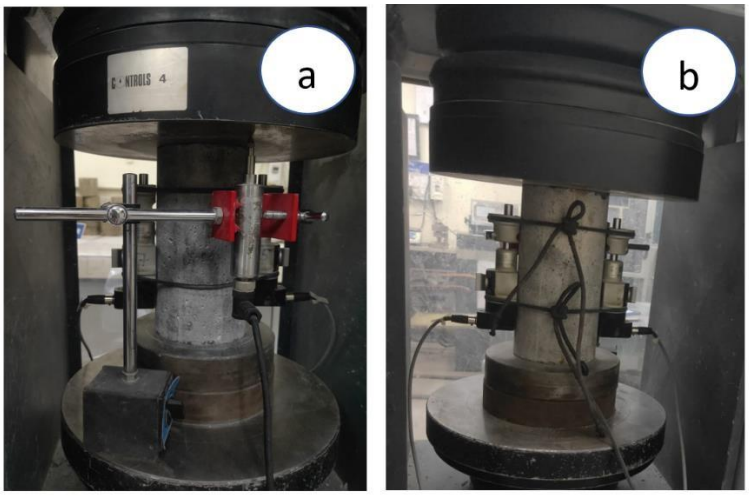

Figure 2. *Testing setup for Stress-Strain Curve (a.) View 1, (b.) View 2*

As can be seen from the figure for recording the strain, one LVDT and two compressometers in different directions are utilized based on the recording channels available in the strain-controlled machine. The Single LVDT and average of two compressometer readings are reported in the study. Although it is recommended to use two LVDTs also in two different directions due to the limitation of the recording channels, an optimum choice of two Compressometers and one LVDT has been made. The choice has been made based on the higher sensitivity of the compressometer as it is directly attached to the specimen. Also, the LVDT is suitable for capturing complete stress-strain response but accuracy is not at par with compressometer due to error coming from platen to platen measurement and larger gauge length. The behavior of compressometer and LVDT in capturing stress-strain response has been discussed in the results and discussion section based on the experimental study done.

4. Results and Discussion

4.1 Compressive strength and failure modes

Compressive strength was tested on cylinders of size 100 x 200 mm. The results of compressive strength for all the mixes are shown in (Figure 2). The maximum value of average compressive strength was observed for Mix 1 and Mix 4 which was approximately 140 MPa and the minimum value was observed for Mix 5 which was 111 MPa. It was observed that the performance of VHSC is very production sensitive i.e. it varies widely and will perform differently in case of little change in the production process which majorly includes a selection of material, mixing methodology, and curing regime. The exceptionally high compressive strength of VHSC may be attributed to high packing density, dense ITZ due to low water binder ratio and unavailability of CH crystals, presence of secondary C-S-H in voids as a result of the pozzolanic reaction. It was observed that for all the seven VHSC mixes, the value of wet packing density (ϕ) was more than 0.8. Such a high value of

DOI: 10.7764/RIC.00046.21

wet packing density indicates that VHSC has a dense microstructure that assists in achieving ultra-high compressive strength. Results indicate that packing density and compressive strength have a direct correlation that is higher wet packing density leads to better performance in compressive strength as shown in (Figure 3).

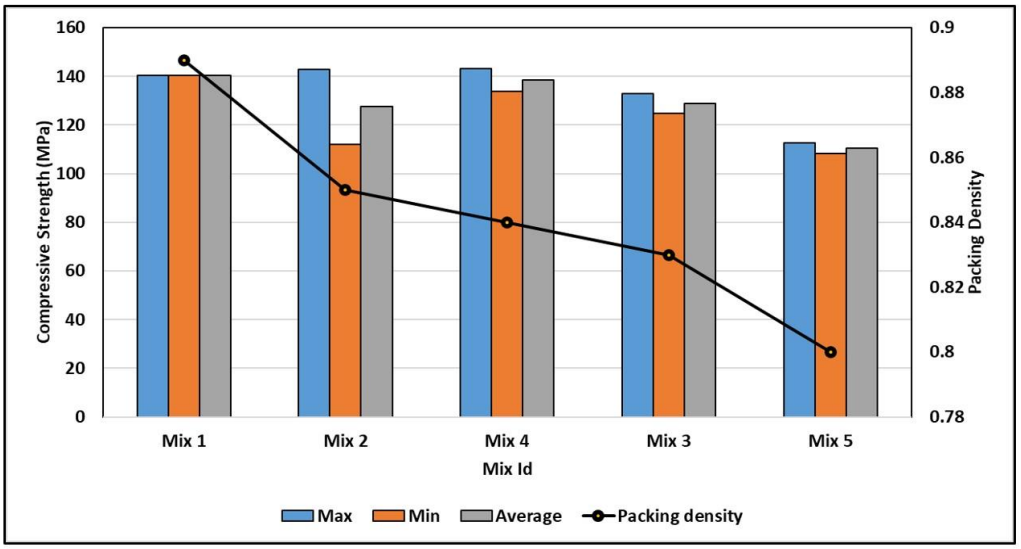

Figure 3. *Compressive strength and packing density of all mixes*

(Figure 3) shows the compressive strength data for the nine specimens considered for stress-strain behavior study arranged in sequence of decreasing packing density. Two samples each for mix 2, to mix 5 were considered and one sample for mix 1 was tested. (Figure 3) shows the maximum, minimum, and average values for the specimens tested along with the packing density for each mix.

Experimental results also indicate that, unlike conventional normal strength concrete which gradually fails after reaching its peak load, the VHSC explodes at peak load similar to the High strength concrete. Typical splitting rupture failure was noticed. The stress-strain behavior of VHSC in compression is more linear than conventional concrete up to its compressive strength, and the fracture of the compressive specimen is more brittle in comparison to conventional concrete.

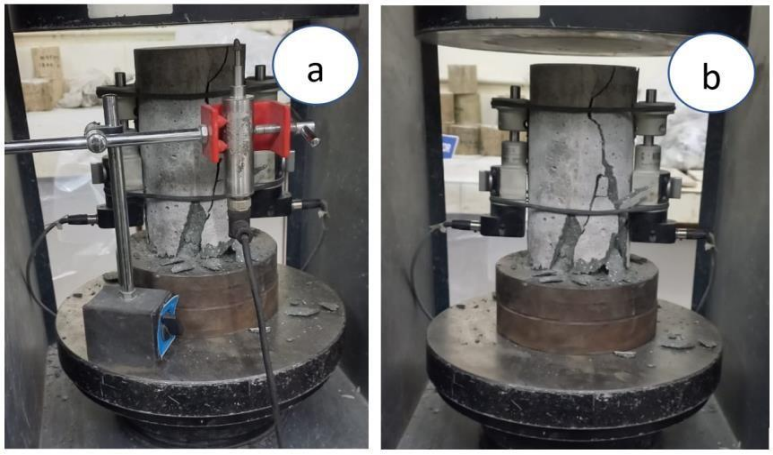

Figure 4. *The failure mode of the tested concrete specimen (a.) View 1, (b.) View 2*

DOI: 10.7764/RIC.00046.21

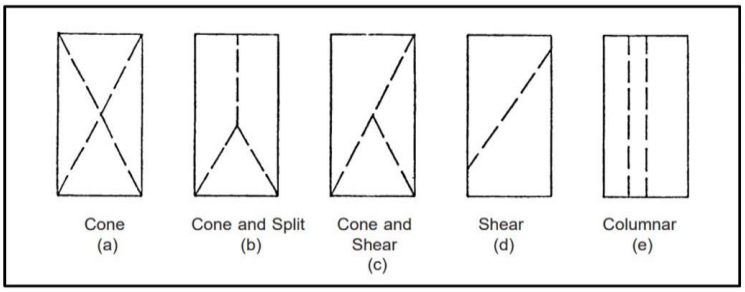

***Figure 5**. Failure modes for cylindrical specimens in compression (ASTM , 2017)*

An image of the broken specimen showing the failure mode is given in (Figure 4) and, the Five distinct typical forms of fracture are shown in (Figure 5) from ASTM C 39-03 (ASTM, 2017). Comparing (Figure 3) with (Figure 4). The obtained failure mode for the tested specimen best resembles with columnar (5e) type of fracture. The cylindrical specimen has been cracked vertically and split into two parts. The obtained failure mode is affected by the friction at the platen ends. When friction between the platens of the testing machine restrains lateral expansion of the concrete and the vertical compressive force is applied, a cone failure occurs. When the cylinder is fractured in this manner, two relatively intact cones are observed (5a). This type of failure is common for normal strength concrete. If, however, the friction were removed or the load applied is too high, compared to acting friction at platen, the cylinder would expand further laterally and divide into two parts vertically resulting in a columnar type of failure (5e), as obtained in the present study for very high strength concrete. Many studies on high-strength specimens made of mortar or pure cement paste have shown vertical splitting, although the result is less prevalent in regular normal strength concrete when a larger coarse aggregate is used (Neville, 1995).

4.4 Stress-Strain Behaviour of VHSC

The findings of the stress-strain behavior study conducted are discussed in the following section and obtained curves are given in (Figure 6(a)). The Figure shows stress-strain behavior for nine individual samples tested and three sets of curves from the literature (Arora et al., 2019) for comparison purposes. Specifically, 4(a) has been taken from the literature (Arora et al., 2019), and (Figure 6 (b)), (Figure 6 (c)), (Figure 6(d)) are obtained experimentally. Each curve consists of two plots – (i.) Strain measured with LVDT vs stress and, (ii.) Strain measured with compressometer vs stress. Details about the color code of the curves are given in the legend at the lower right corner of each plot. For each of the plot strain values, maximum stress is given near the maximum stress coordinate and maximum stress is given in the legend.

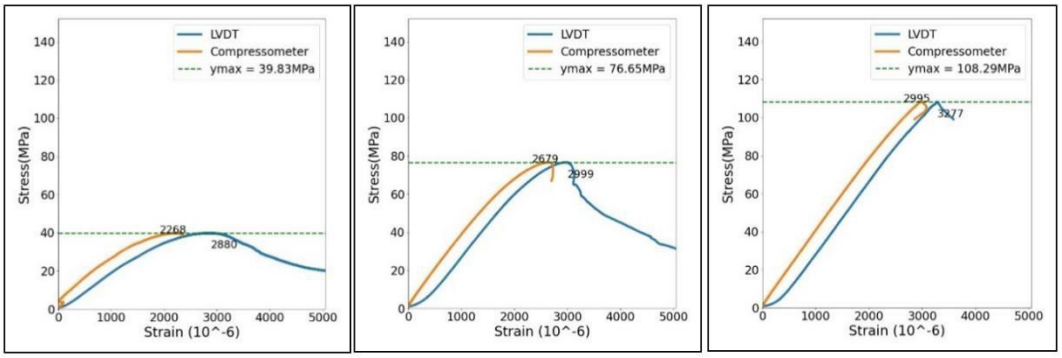

***Figure 6(a).** Normal, High and very high Strength Concrete (Arora et. al., 2019)*

DOI: 10.7764/RIC.00046.21

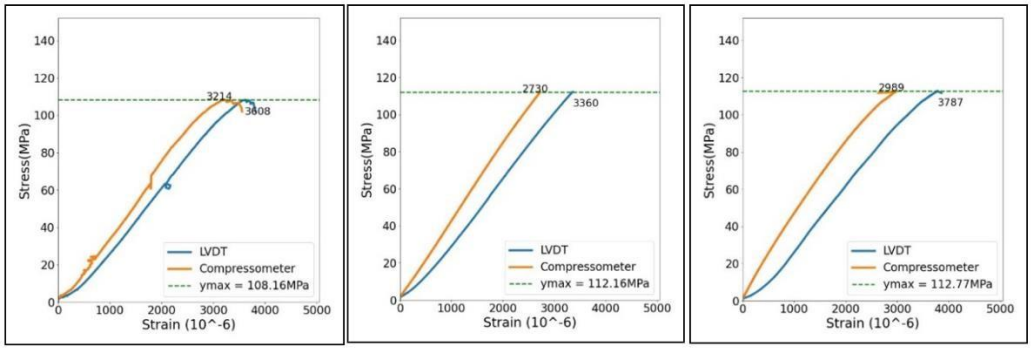

Figure 6(b). *Very High Strength concrete of 100 MPa to 120 MPa Compressive strength*

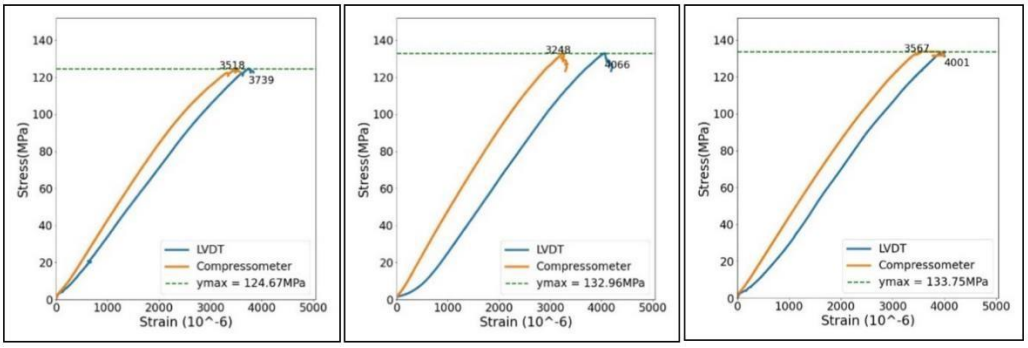

Figure 6(c). *Very High strength concrete of 120 MPa to 140 MPa Compressive strength*

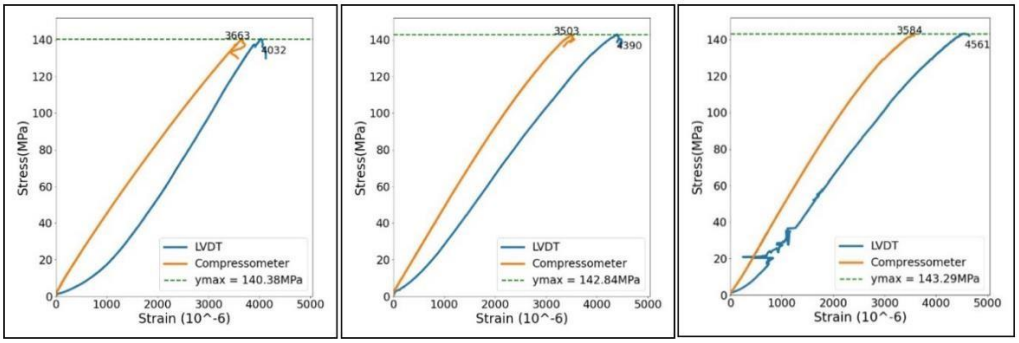

Figure 6(d). *Very High strength concrete with More than 140 MPa Compressive strength*

In (Figure 6(a)) the stress-strain curves for concrete with compressive strength of 40 MPa show a significant zone of strain hardening. Similar behavior of the concrete has been adopted in IS 456 where the concrete is assumed to have a distinct strain value for peak stress and ultimate stress. (Figure 8) shows the assumed stress-strain characteristics in IS 456. As shown in (Figure 8), IS 456 assumes strain at ultimate stress and ultimate strain as 2000 micro strains and 3500 microstrains respectively.

DOI: 10.7764/RIC.00046.21

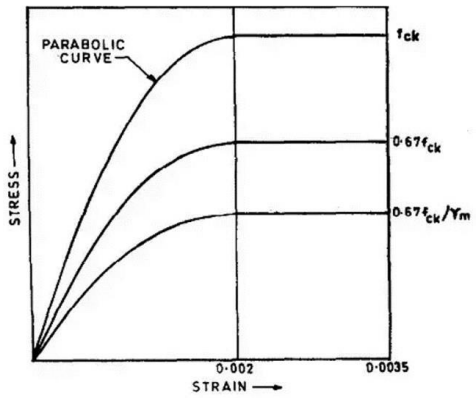

Figure 7. *Standard Stress-strain characteristics of concrete are defined by IS 456 (Bureau of Indian Standards,2000)*

The assumed behavior of the concrete in IS 456 does not hold well for higher strength concrete in two ways. First, the constant strain values adopted in IS 456 are not suitable for different strength ranges of high strength concrete and second, the assumed parabolic behavior does not apply to higher strength concrete. As observed in curves 4(b), 4(c), and 4(d), the strain at the peak stress and strain and the failure coincide for concrete with compressive strength above 100 MPa. The material failed just after reaching the ultimate stress and a significant zone of strain hardening is not observed. Also, the strain at peak stress for concrete with compressive strength of 100 MPa to140 MPa is between 3000 microstrains to 3600 microstrains, as captured by the compressometers. Instead of a parabolic curve up to ultimate stress, a straight line will better describe the stress-strain behavior of high-strength concrete. Literature (Baduge et al., 2018), (Al-Zwainy et al., 2016) also suggests that with the increase in the compressive strength of concrete the initial parabolic curve tends to assume a straight line. Past studies done by (Arora et al.,2019) as shown in (Figure 6(a)) show a transition of curves from concrete compressive strength of 40 MPa to 100 MPa. The transition clearly shows the appearance of linearity in the rising limb of the curves with the increase in the compressive strength. The findings of the present study follow the trend. Also, in the curves for 40 MPa and 76 MPa in (Figure 6(a)), the LVDT gives a zone of strain hardening after the peak stress which disappears for concrete with compressive strength above 100 MPa. This behavior is also magnified by the findings in the present study. All the specimens failed after reaching the ultimate stress as anticipated from the literature (Baduge et al., 2018), (Al-Zwainy et al., 2016).

Table 5. *Comparison of Stress-strain characteristics of Normal, High, and very-high strength concrete*

Strength Category	Peak stress (MPa)	Average Stress (rounded to a multiple of 10) (MPa)	Strain at peak stress (micro-strain)	Average Strain (micro-strain)	EC:02-2004	IS456
Normal strength concrete	39.83 [20]	40	2268	2268	2000	2000
High strength concrete	76.65 [20]	80	2679	2679	2488	Only up to M55
Very high strength concrete (100-120MPa)	108.29 [20]	110	2995	2982	Only up to 90 MPa	
	108.16		3214			
	112.16		2730			
	112.77		2989			
Very high strength concrete (120-140 MPa)	124.67	130	3518	3444		
	132.96		3248			
	133.75		3567			
Very high strength concrete (>140 MPa)	140.38	140	3663	3583		
	142.84		3503			
	143.29		3584			

DOI: 10.7764/RIC.00046.21

(Table 5) presents a summary of the plots given in (Figure 6) and compares it with IS: 456 -2000 and EC-02 -2004. As presented in the table both the codal provisions does not cater concrete above 100 MPa of compressive strength. The past study (Arora et al., 2019) gives strain at peak stress value for Concrete with strength of 40 MPa to be 2268 micro-strains which increased to 3583 micro-strains for 140 MPa compressive strength in the present study. The table shows an 158% increase in recorded strain for 350% increase in the compressive strength between 40 MPa to 140 MPa.

4.5 Strain measurement

For measuring the strains different types of instruments can be used. These include compressometer, LVDT, strain gauges, etc. These instruments use different gauge length ratios and these gauge length ratios impart a significant effect on the recorded stress-strain curves. Gauge length ratio is defined as the ratio of gauge length to the length of the specimen. The instruments with smaller gauge length ratios show a more ductile stress-strain behavior. This is due to more sensitivity of the larger gauge length ratio towards the generated cracks in the specimen, as it covers a larger part of the specimen compared to the smaller gauge length ratios. In the present study, LVDT and compressometer are used. These two uses different gauge length ratio. LVDT has a gauge length ratio of 1 for all the mixes. Whereas the compressometer uses a gauge length of 0.45 for all the mixes. The effect of variation of gauge length ratios is visible on the obtained stress-strain curves. The compressometer with a lower gauge length ratio than LVDT is showing a steeper slope than LVDT in the recorded stressstrain curves. For the strain measurement using LVDT the platen to platen, measurement is done. This has a significant impact on the stress-strain behavior captured by the LVDT. But the platen-to-platen measurement is generally suggested for the higher strength concrete because it can capture the cracks in the entire height of the specimens.

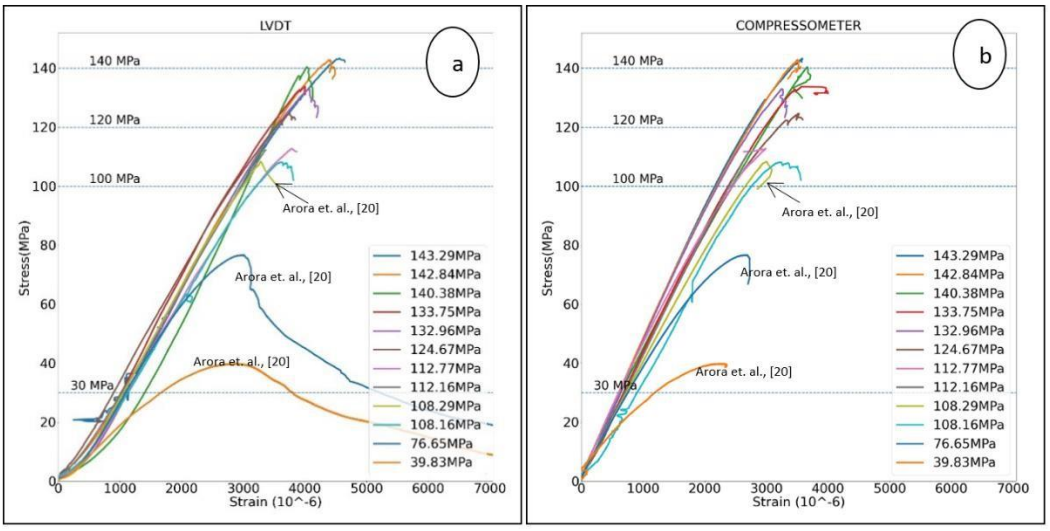

Figure 8. *(a)Combined graphs for Strain (LVDT) vs stress (b)Combined graphs for strain (Compressometer) vs stress*

(Figure 8(a)) and (Figure 8(b)) show the combined curves for the stress vs strain (LVDT) and stress vs strain (compressometer) for all the specimens. In both the figures, we observe that with the increase in the compressive load the curves get steeper with the increase in the compressive strength. In (Figure 8(a)) and (Figure 8(b)) we also observe an approximately ideal straight line for the higher strength concrete. This result aligns with the previous findings in the literature which suggests this trend with an increase in strength. (Singh et al., 2020) had suggested that the ideal stress-strain curves for concrete up to M55 in IS: 456 will not hold well for higher strength concrete up to M90. They assumed a straight-line curve instead of a parabolic for higher strength. The suggested modification holds good for higher strength concrete. With the increase in strength, the stress-strain behavior of concrete, up to peak stress can be safely assumed to be a straight line. A comparison of the strain values recorded from the LVDT and the compressometer is given in (Table 6).

DOI: 10.7764/RIC.00046.21

Table 6. *Comparison of strain values recorded by LVDT and Compressometer*

Stress	LVDT	Compressometer	Difference (% Compressometer)
108.16	3608	3214	12.26
112.16	3360	2730	23.08
112.77	3787	2989	26.70
124.67	3739	3518	06.28
132.96	4066	3248	25.18
133.75	4001	3567	12.17
140.38	4032	3663	10.07
142.84	4390	3503	25.32
143.29	4561	3584	27.26

As discussed above, LVDT and compressometer record slightly different values. The recorded strain in the LVDT is 10 % to 25 % higher than the corresponding strain value recorded in the compressometer. The variation of the recorded strain value between the LVDT and the compressometer of for peak stress of 112.6 MPa is 23%. Similar variation is obtained for peak stress level of 132 MPa, 142 MPa and 143 MPa with lesser variations in between. Therefore, it can be inferred that recorded strain values differ randomly and no relation with the peak stress applied can be established. Similar variation has been reported by past study (Arora et al., 2019), where compressometer reported smaller strain values than the LVDT by 10% to 20% for normal and high strength concrete.

5. Conclusion

The key to the production of VHSC, which demands both a low w/binder ratio to be used and high workability to be attained, is the maximization of the packing density of the granular skeleton of the concrete. With the help of the Modified Andreasen and Andersen equation, different combinations of solid material have been optimized to produce VHSC with high compressive strength. VHSC is production sensitive materials i.e. its properties vary widely with a small change in the production process. The use of a high energy mixer is vital for high mixing efficiency and homogeneous mixing of VHSC without any lump formation which enhances its properties in the fresh and hardened state. To develop VHSC with a high amount of mineral admixture, the curing regime also plays a very important role. Post-set heat treatment enhances the microstructure by speeding up the pozzolanic reaction of Silica fume and other ultrafine cementitious materials to enhance the mechanical properties. The results from the stress-strain study can be concluded as follow:

A. *A change in compressive strength changes the stress-strain behavior of the concrete drastically. For strength rise from 40 MPa to 80 MPa strain at peak stress increased by 18%. Where for the strength 110MPa,130MPa, and 140MPa the increase is 31%, 52%, and 58% of the strain values for concrete with 40MPa strength.*
B. *The stress-strain curves obtained gets steeper with an increase in the strength of the concrete. Also at a higher strength, the curves follow a straight-line path contrary to the parabolic path for normal and some extent for high strength concrete.*
C. *With the increase in strength of the concrete, post-peak behavior shrinks and finally coincides with very high strength concrete. This results in the approximately equal strain at peak stress and ultimate strain at failure.*
D. *The decrease in ultimate strain and increase in strain at peak stress of high to very high strength concrete will have a direct impact on the depth of the neutral axis for a balanced section which is directly related to the maximum capacity of the member*

E. *LVDT and compressometer give slightly different strain values for the same load and same concrete material. This is due to the difference in the gauge length ratio used in these strain measuring devices. compressometer is incapable of capturing the post-peak behavior of the concrete, whereas LVDT shows errors at the starting of the loading in the experiment.*

6. Acknowledgements

The authors acknowledge the funding received from the Ministry of Commerce & Industry, Govt. of India.

7. References

Al-Zwainy, F.M.; Risan, H.; Zaki, R. (2016). Meta-analysis of fiber impact on mechanical properties of ultra-high performance concrete," Ciência e Técnica Vitivinícola, vol. 31, pp. 101–113, Apr. 2016.

Arora, V.V.; Singh, B.; Jain, S. I. (2016). "Experimental studies on short term mechanical properties of high strength concrete" Concrete Journal, Vol. 90, No. 10, pp. 65-75, October 2016.

Arora, V.V.; Singh, B.; Jain, S. (2017). Effect of indigenous aggregate type on mechanical properties of high strength concrete Indian Concrete Journal, Vol. 91, No. 1, pp. 34-44.

Arora, V.V.; Singh, B.; Patel, V. Mohapatra, B.; Daniel, Y. (2019). Stress-Strain Behaviour And Performance Evaluation Of High Strength Steel Fibre Reinforced Concrete (Sfrshc). Indian Concrete Journal. 93. 54-61.

Arora, V.V.; Singh, B.; Patel, V.; Trivedi, A. (2020). Evaluation of modulus of elasticity for normal and high strength concrete with granite and calc-granulite aggregate. Structural Concrete, vol. 22, no. S1. Wiley, Jul. 16, 2020. doi: 10.1002/suco.202000023.

ASTM (2017). C39/C39M-03 Standard Test Method For Compressive Strength Of Cylindrical Concrete Specimens. USA: ASTM.

Attard, M. M.; Stewart, M. G. (1998) Two parameter stress block for high-strength concrete ACI Structural Journal 95(3): pp. 305–317

Baduge, K.; Shanaka, et al. (2018). Stress-Strain Relationship for Very-High Strength Concrete (>100 MPa) Confined by Lateral Reinforcement. Engineering Structures, vol. 177, pp. 795–808. DOI.org (Crossref), https://doi.org/10.1016/j.engstruct.2018.08.008.

Bureau of Indian Standards (BIS) (2000). IS 456: 2000 Reinforced Concrete - Code Of Practice," Indian Standards.

Campos, H.F.; Klein, N.S.; Marques Filho, J. (2020)."Proposed mix design method for sustainable high-strength concrete using particle packing optimization, Journal of Cleaner Production, vol. 265. Elsevier BV, p. 121907, doi: 10.1016/j.jclepro.2020.121907.

Chan, Y.W.; Chu, S.H. (2004). Effect of silica fume on steel fiber bond characteristics in reactive powder concrete, Cem. Concr. Res. 34 (7) 1167–1172.

De Larrard, F.; Sedran, T. (1994). Optimization of ultra-high-performance concrete by the use
of a packing model. Cem Concr Res 24(6):997–1009.

European Standards EN (2004). BS EN 1992-1-1:2004. Eurocode 2: Design of Concrete Structures. General Rules and Rules for Buildings.

Habeeb, M.; Al-Azzawi, A.A.; Al-Zwainy, F. (2019). Punching shear behaviour of solid and bubble reinforced light Weight aggregate concrete two-way slabs," in IOP Conference Series: Materials Science and Engineering, vol. 584, no. 1. doi: 10.1088/1757-899X/584/1/012013.

Habeeb, M.; Al-Azzawi, A.A.; Al-Zwainy, F.M.S. (2021). Punching shear behavior of LWA bubble deck slab with different types of shear reinforcement," Journal of King Saud University - Engineering Sciences, vol. 33, no. 1, doi: 10.1016/j.jksues.2020.01.001.

Kwan, A. K. H., et al. (1995). Development of Very High Strength Concrete for Hong Kong." HKIE Transactions, vol. 2, no. 2, pp. 9–16. DOI.org (Crossref), https://doi.org/10.1080/1023697X.1995.10667681. **Neville, A. (1995)** Properties of Concrete, 4th ed. Prentice Hall.

Norzaireen, M. A.; Nasir, Shafiq (2018). Ultra-High Performance Concrete: From Fundamental to Applications", Case Studies in Construction Materials

Ojha, P.N.; Singh, B.; A. Singh, A.; V. Patel, V. (2020). Comparison of creep models and experimental verification of creep coefficients for normal and high strength concrete," Journal of Asian Concrete Federation, vol. 6, no. 2. Asian Concrete Federation, pp. 24–36. doi: 10.18702/acf.2020.12.6.2.24.

Ojha, P.N.; Mittal, P.; Singh, A.; Singh, B.; Arora, V.V. (2020). Optimization and Evaluation of Ultra High Performance Concrete, Asian Concrete Federation Journal, Volume 6, No.1, June 2020, pp 26-36.

Ojha, Parmanand; Singh, Brijesh; Singh, Abhishek; Patel, Vikas; Arora, V.V. (2021). Experimental study on creep and shrinkage behavior of high strength concrete for application in high rise buildings. Indian Concrete Journal. 95. 3042.

Oztekin, E.; Pul, S.; Husem M. (2003). Determination of rectangular stress block parameters for high performance concrete" Engineering Structures, Vol. 25, pp. 371-376

Patel, Vikas; Singh, Brijesh; Arora, V.V. (2020). Study on Fracture Behavior oF high Strength concrete including eFFect oF Steel FiBre. Indian Concrete Journal. 94.

Richard, P.; Cheyrezy, M. (1995). Composition of reactive powder concretes, Cem.e Concr. Res. 25 (7) 1501–1511.

Riedel, P.; Leutbecher, T.; Piotrowski, S.; Heese, C. (2019). Ratios of Compressive Strengths of Ultra-High-Performance Concrete Specimens of Different Shapes and Sizes. ACI Materials Journal, vol. 116, no. 6, doi: 10.14359/51716983.

Singh, B. et al., (2021). Empirical equation and experimental validation of shear parameters for high strength concrete (HSC)," The Journal of Asian Concrete Federation, vol. 7, no. 2. Asian Concrete Federation, pp. 46–55. doi: 10.18702/acf.2021.12.7.2.46.

Singh, B.; Arora, V.V.;Pate l, V. (2020). Experimental study on stress strain behaviour of normal and high strength unconfined concrete. Indian Concrete Journal, Vol. 94, No. 4, pp. 10-19, , NCCBM, Haryana, India.

Singh, B.; Ojha, P.; Trivedi, A.; Patel, V.; Arora, V.V. (2021). Development Of Empirical Equations For Prediction Of Flexural And Split Tensile Strength For Normal And High Strength Concrete With Granite And Calc-Granulite Aggregate. Indian Concrete Journal. 95. 36-46.

Singh, B.; Patel, V.; Ojha, P.N.; and Arora, V.V. (2020). Analysis of stress block parameters for high strength concrete, Journal of Asian Concrete Federation, vol. 6, no. 1. Asian Concrete Federation, pp. 1–9. doi: 10.18702/acf.2020.6.6.1.

Singh, B.; Patel, V.; Ojha, P.N.; Trivedi, A. Arora, V.V. (2022). Experimental Shear Study on Reinforced High Strength Concrete Beams Made Using Blended Cement. Journal of Architectural Environment & Structural Engineering Research, vol. 5, no. 1. Bilingual Publishing Co. doi: 10.30564/jaeser.v5i1.4064.

Shi, C. (1996). Strength, pore structure and permeability of alkali-activated slag mortars, Cem. Concr. Res. 26 (12) 1789–1799.

Schmidt, M.; Fehling, E. (2007). Grundlagen der Betontechnologie von Hochund Ultra Hochleistungsbeton und Anwendung von UHPC im Bruckenbau, in: Ultra High Performance Concrete – 10 Years of Research and Development at the University of Kassal, Kassel, Germany, pp. 70–81.

Sorelli, L.; Constantinides, G.; Ulm, F.J. et al., (2008). The nano-mechanical signature of ultra high performance concrete by statistical nanoindentation techniques, Cem. Concr. Res. 38 (12) 1447–1456.

Zeng, Jun-Jie, et al. (2020). Stress-Strain Behavior of Polyethylene Terephthalate Fiber-Reinforced Polymer-Confined Normal-, High- and Ultra High-Strength Concrete. Journal of B*uilding Engineering, vol. 30, p. 101243. DOI.org (Crossref), https://doi.org/10.1016/j.jobe.2020.101243.*